ACS APPLIED MATERIALS & INTERFACES

Research Article

www.acsami.org

Nanopatterning of a Stimuli-Responsive Fluorescent Supramolecular Polymer by Thermal Scanning Probe Lithography

Samuel Tobias Zimmermann,[†,∥] Diederik W. R. Balkenende,[‡,§,∥] Anna Lavrenova,[‡] Christoph Weder,[*,‡] and Jürgen Brugger[*,†]

[†]Microsystems Laboratory, École Polytechnique Fédérale de Lausanne, CH-1015 Lausanne, Switzerland

[‡]Adolphe Merkle Institute, University of Fribourg, 1700 Fribourg, Switzerland

Supporting Information

ABSTRACT: The miniaturization of nanometer-sized multicolor fluorescent features is of continuous significance for counterfeit security features, data storage, and sensors. Recent advances in engineering of stimuli-responsive supramolecular polymeric materials that respond upon exposure to heat or mechanical force by changing their fluorescence characteristics open new opportunities as functional lithographic resists. Here, we demonstrate the patterning of a thermochromic supramolecular material by thermal scanning probe lithography (t-SPL), an emerging nanofabrication technique, which allows for ultrafast indentation with a heated probe, resulting in both fluorescent and topographic nanofeatures. t-SPL indentation reveals a linear relationship between the temperature at which material softening occurs and the indentation force in the range from 200 to 500 nN. The softening temperature decreases as the heating time increases from 4 μs to 1 ms, following time−temperature superposition behavior. Our results herein confirm that the fluorescence contrast, perceivable as a shift from red to green, was obtained by kinetic trapping of the dissociated state due to ultrarapid cooling when the probe is removed. We use t-SPL to create highly customized fluorescence patterns up to 40 × 40 μm^2 in size with a spatial resolution of 86 nm and change the pitch size to modify the fluorescence intensity when observed by fluorescence microscopy. As an application, multifaceted security features with nanometer resolution are explored.

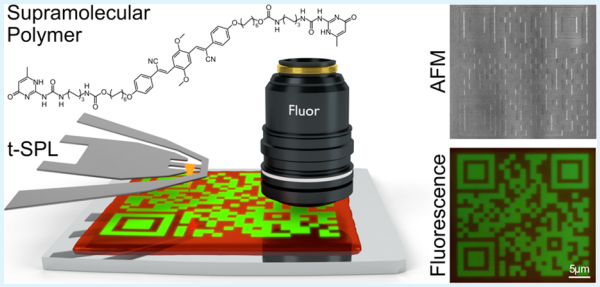

KEYWORDS: *supramolecular polymer, thermoresponsive luminescence, thermal scanning probe lithography, nanopatterning, anticounterfeiting*

INTRODUCTION

Thermal scanning probe lithography (t-SPL) is a method that enables nanoscale patterning through the interaction of a heated probe in contact with a substrate material.[1] The heat transferred from the tip to the substrate induces physical and/or chemical modifications in a target material, which are delimited to the tip−substrate contact area, typically on the order of a few tens of nanometers in diameter. While the technology was initially developed for data storage, t-SPL has become an emerging lithography method for nanopatterning of temperature-sensitive and functional materials, such as polymers,[2,3] graphene oxide,[4] molecular glasses,[5] metal alloys,[6] and semiconductors.[7−9] Closed-loop lithography, a key feature of t-SPL, enables thermal patterning of a substrate material with the tip being heated and in situ recording of the surface topography with the tip being at room temperature. This enables rapid prototyping of three-dimensional (3D) patterns into temperature-sensitive resists,[2,3] which can subsequently be transferred into silicon or used for lift-off.[10−12] Chemical reactions, triggered by the heated probe in contact with the substrate surface, enable nanoscale functional patterns, such as electrically conducting reduced graphene oxide[4] or semiconducting photoluminescent poly(*p*-phenylenevinylene) nanostructures.[7,8] t-SPL is not limited to organic materials and has been applied on GeTe phase change materials to create crystalline, electrically conductive, and optically absorptive nanoscale patterns from an amorphous, transparent, and electrically insulating substrate.[9] In comparison to laser-assisted nanoimprint lithography[13] or ultrafast thermal nanoimprint lithography,[14] t-SPL is a digital patterning technique which does not require a mask.

Supramolecular polymer glasses are an emerging category of stimuli-responsive materials that exhibit a high elastic modulus at room temperature in the solid state.[15−17] These materials can be converted into low-viscosity liquids when heated above their glass transition temperature (T_g), on account of the thermally driven, reversible disassembly into the parent low-molecular-weight building blocks.[18] These materials find applications in the field of sensing[19] and self-healing.[20] The concept of supramolecular polymer glasses has been recently extended to

Received: September 10, 2017
Accepted: October 27, 2017
Published: October 27, 2017

DOI: 10.1021/acsami.7b13672
ACS Appl. Mater. Interfaces 2017, 9, 41454−41461

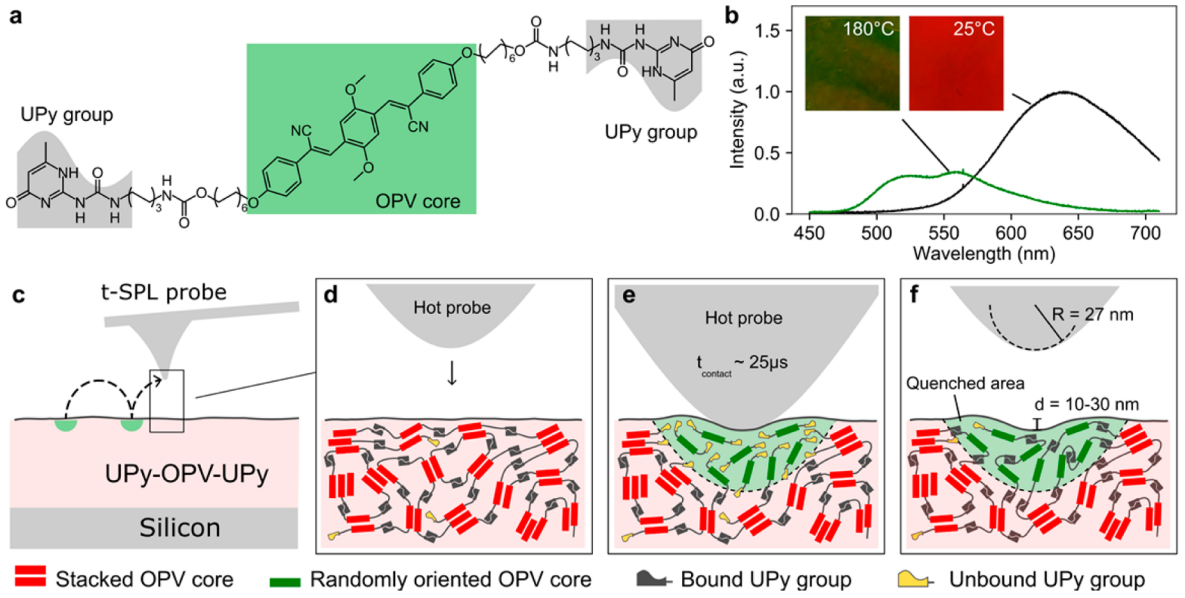

Figure 1. Nanolithography with a color-switchable fluorescent supramolecular polymer resist. (a) The chemical structure of the UPy–OPV–UPy building block is shown, with the excimer-forming fluorescent OPV core and the supramolecular UPy binding motifs highlighted. (b) Fluorescence spectra of a bulk sample of UPy–OPV–UPy at 180 and 25 °C. The inset shows pictures of the fluorescing sample under UV illumination. (c) Schematic representation of the single-step fabrication of multicolor patterns using thermal scanning probe lithography. (d) Illustration of the polymer film topography and molecular assembly, with the OPV cores aggregated in excimer-forming stacks and the UPy binding motifs dimerized. (e) Indentation with a hot t-SPL probe locally liquefies the material and disassembles the building blocks, which results in a green fluorescence. (f) Upon rapid probe removal, the high-temperature state is quenched so that a green fluorescing area is retained.

mechanoresponsive luminescent (MRL) and thermoresponsive luminescent (TRL) supramolecular polymers by synthesizing a MRL/TRL dye with supramolecular binding motifs. Self-complementary hydrogen-bonding ureido-4-pyrimidinone (UPy) groups were used to promote the self-assembly[21] of an excimer-forming cyano-substituted oligo(*p*-phenylenevinylene) (cyano-OPV) derivative[22−24] into a supramolecular polymer (UPy–OPV–UPy, Figure 1a).[25] This material has the following characteristics: (i) it can be readily molded into self-supporting objects of various shapes, (ii) it displays the thermomechanical characteristics of a supramolecular polymer glass, (iii) it offers three different emission colors in the solid state, and (iv) it exhibits both MRL and TRL behavior on account of stimuli-induced modification of the molecular packing, which in turn impacts the material's emission characteristics (Figure 1b).[25] While the ability to control the fluorescence color of blends of cyano-OPVs and glassy amorphous polymers via the extent of dye aggregation was exploited before in three-dimensional optical data storage systems, heat-transfer processes did not permit a voxels with dimensions of less than a few micrometers.[26] The resolution of two-photon laser-induced aggregate switching is limited to a few micrometers due to the diffraction-limited spot size and lateral heat transfer during exposure. In a more recent publication, a quaternary data storage system using thermoresponsive cyano-OPV and a photoresponsive dye in a polymer matrix was proposed to create a material selectively responsive to heat and light.[27] While this material allowed four different colors to be obtained under activation with light, heat, or a combination of both, the resolution was limited to 200–300 μm. To overcome such limitations in resolution, we exploit the capability of t-SPL to apply extremely fast heating rates on the order of 10^7 K/s. In addition, we exert simultaneously well-controlled mechanical forces in the range of 200–500 nN at the probe–sample contact point. This concept is demonstrated by reversibly switching the state of assembly and therewith the fluorescence characteristics of UPy–OPV–UPy under extremely short heat and force pulses created by a heated t-SPL probe (Figure 1c–f). It is hypothesized that kinetic trapping of the green fluorescent high-temperature OPV dissociated state is facilitated due to short contact and fast heat dissipation after the heated probe is removed. We present results on atomic force microscopy (AFM) force spectroscopy of UPy–OPV–UPy films, nanoindentation and nanopatterning by t-SPL, and the maximum achieved resolution, and demonstrate topographic/fluorescent images as an example of anticounterfeiting nanosystems.

MATERIALS AND METHODS

UPy–OPV–UPy was synthesized as previously described and an in-depth structural characterization of the molecule is recently reported.[9] Films for our studies were fabricated by melting UPy–OPV–UPy in powder form on a silicon chip mounted on a hot plate at 180 °C and doctor-blading the hot melt over the substrate. The samples were then cooled under ambient conditions (1.3 °C/s) to room temperature, thus allowing sufficient time for the cyano-OPV moieties to aggregate into their thermodynamically favored stacked arrangement. As expected, cooling was accompanied by a fluorescence shift from green to red owing to the aggregation of cyano-OPV as depicted in the spectra and images in Figure 1b. The thickness of the resulting films was 20 ± 10 μm, as measured by a mechanical profilometer (Alpha-Step 500, KLA-Tencore, USA). The large deviation in film thickness between different films originates from the manual fabrication and could be improved by using a hot-press with pressure control at the expense of the simplicity of the manual coating. Despite the occurrence of thickness variations on the order of hundreds of nanometers over the entire sample, the surface of the films was smooth over an area relevant for t-SPL. A typical root-mean-square surface roughness of 5.7 ± 3.0 nm was measured over an area of 50 × 50 μm^2.

Before t-SPL experiments are performed and to determine the thermomechanical properties of UPy–OPV–UPy films, we performed AFM force spectroscopy on heated samples using a Nano Wizard II

DOI: 10.1021/acsami.7b13672
ACS Appl. Mater. Interfaces 2017, 9, 41454–41461

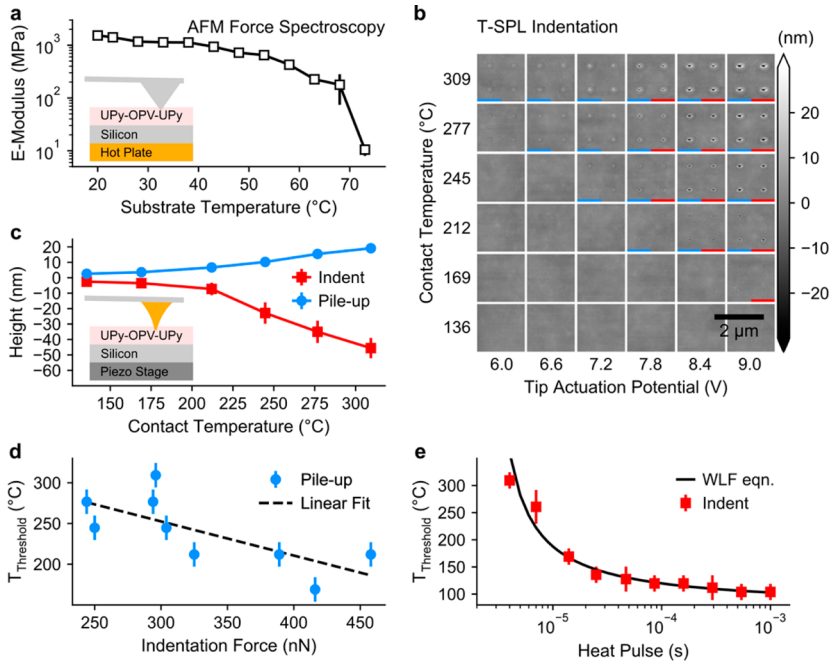

Figure 2. Thermomechanical indentation of the TRL supramolecular polymer. (a) The elastic modulus of 20 ± 10 μm thick UPy−OPV−UPy films obtained from AFM-based force spectroscopy is plotted against the sample temperature. The inset depicts the experimental setup. (b) AFM topography images obtained from t-SPL indentation by varying the tip temperature between 130 and 310 °C and the indentation force between 200 and 500 nN (tip actuation potential 6.0−9.0 V). The colored bars indicate whether an indent was formed (red) or a pileup (blue). (c) The indentation depth and height of the pileup around the indent from thermomechanical indentation with a hot probe are plotted against the tip temperature. (d) The threshold temperature above which an indent or a pileup is formed is plotted against the indentation force and fitted with a linear function. (e) The temperature threshold to form an indent is plotted against the heating time and fitted using the Williams−Landel−Ferry equation for a constant tip actuation potential of 7.8 V.

AFM tool (JPK Instruments AG, Germany) equipped with a cantilever for nanoindentation (DNISP, Bruker AFM Probes, USA) and a heating stage (HTHS, JPK Instruments AG, Germany). The samples were heated from 20 to 75 °C as monitored with an Optris PI infrared camera. Between each temperature change, enough time was given for the UPy−OPV−UPy film to thermally equilibrate until the temperature reached a steady state. An indentation depth of 30 nm was targeted for the AFM force spectroscopy measurements on the bulk-heated sample so that it matches typical values used hereafter in t-SPL. The force−distance curves were analyzed (JPK Software) and all force spectra were corrected for cantilever deflection. The unloading part of the force−distance curves were fitted (upper 50% of the curve) and analyzed according to the Hertz theory to obtain the elastic modulus.

After the nanoindentation experiments with a cold probe and the sample on a hot plate, we now shift to the t-SPL tool and perform experiments with a heated probe on a sample stage that is kept at room temperature. t-SPL was carried out using a commercial tool (NanoFrazor, SwissLitho AG, Switzerland), which controls a silicon cantilever (Frazor-HPL1, Swisslitho AG, Switzerland) with an integrated heater in close proximity to the tip for thermal patterning. UPy−OPV−UPy-coated silicon chips were mechanically clamped to the X−Y piezo positioning stage of the tool with a metallic pin, which served as an electrical contact required for electrostatic actuation of the cantilever to exert the local force between probe and substrate. The governing patterning parameters for the t-SPL process, temperature, force, and heating time were investigated for UPy−OPV−UPy by consecutive variation of a single parameter in a series of experiments as shown in Figure 2. The material response was determined by scanning the patterned surface and evaluating the depth of the indent and the height of the rim formed around the indent (pileup). A script was written that computes the average depth of the indents and the height of the pileup from the AFM topography scan (Supporting Information). The t-SPL tool was operated in pulsed heating mode, whereby the heating of the tip occurred only shortly before and during contact with the substrate; this procedure increases the tip lifetime and also the thermal patterning reliability on the supramolecular glass. Typical settings for heat pulses and electrostatic force pulses were 5−20 and 5−10 μs, respectively. The patterning speed was varied between 200 and 800 μm/s. The temperature at the tip−sample contact is not a priori known because of a reduced heat transport from the resistive heater to the conical tip, which is due to radiative and convective losses, phonon scattering, and an unknown thermal contact resistance at the interface.[28] To estimate the temperature at the tip−sample interface, we used a heating efficiency of 0.25 between the heater and the substrate ($T_{contact} = 0.25(T_{heater} - T_{RT}) + T_{RT}$).[28,29] The heater temperature is computed by the software of the t-SPL tool by fitting the knee point of the measured current−voltage curve with the theoretical value for doped silicon.[30] The indentation force of the t-SPL probe, which was electrically actuated, was calibrated by a procedure described in the Supporting Information. Optical fluorescence microscopy images were acquired with an Olympus BX51 microscope, equipped with a mercury lamp at a wavelength of 365 ± 15 nm (I-line) as an illumination source and the emission was detected at wavelengths larger than 420 nm. The illumination intensity of the fluorescence microscope was carefully adjusted to a level where no bleaching occurred. The optical contrast of fluorescence images was normalized by means of an editing program (GIMP, www.gimp.org), for better visibility. All written t-SPL patterns were labeled by an adjacent pattern to be clearly visible by optical microscopy for identification during fluorescence microscopy (Figure S3). It has to be noted that the fluorescence imaging is diffraction-limited (to about 310 nm), and patterns written with the t-SPL, which are smaller than 310 nm can only be resolved in detail by techniques such as AFM.

RESULTS AND DISCUSSION

While thermomechanical properties, such as the temperature-dependent elastic modulus and the glass-transition temperature, for relatively thick (2 mm) UPy−OPV−UPy films have been discussed in a previous publication,[25] no thermomechanical

DOI: 10.1021/acsami.7b13672
ACS Appl. Mater. Interfaces 2017, 9, 41454−41461

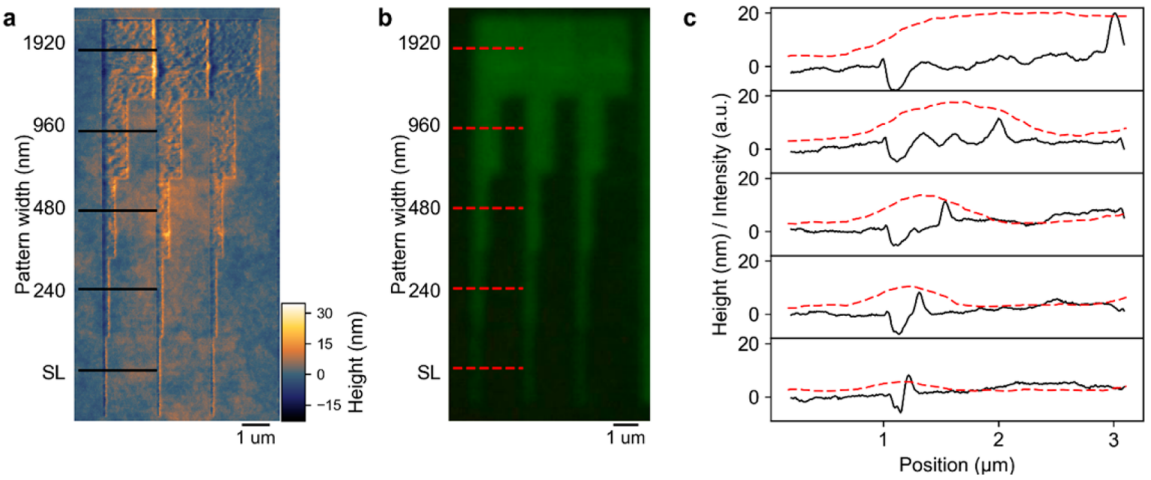

Figure 3. Comparison of the resolution achieved by t-SPL patterning of the color-switchable fluorescent UPy−OPV−UPy and optical readout with a fluorescence microscope. (a) AFM topography image of patterns that were written with t-SPL with features ranging from a single line (86 ± 6 nm) to 1920 nm in width. (b) Fluorescence microscopy image of the same patterns acquired under irradiation with UV light. (c) Profiles extracted from the surface topography image (solid black) and the fluorescence intensity image (dashed red) along the fast scan direction in (a) and (b), respectively.

data is available for nanoindentation of melt-processed films and fast heating rates as achievable in t-SPL. Since the tip temperature in t-SPL is not a priori known and the tip geometry is not well-defined, we perform both conventional AFM force spectroscopy and t-SPL as a comparison to determine the thermomechanical properties of the supramolecular polymer. The elastic modulus of UPy−OPV−UPy films measured by AFM-based force spectroscopy is shown in Figure 2a as a function of the substrate temperature. An elastic modulus of 1.5 ± 0.2 GPa is measured at 20 °C. The modulus linearly decreases with increasing substrate temperature until 68 °C is reached, where it sharply drops by a factor of 20 to 10.5 ± 2.5 MPa. Above 73 °C, indentation experiments were no longer possible due to adhesion of the viscous melt to the tip. The data mirror the results of measurements on bulk UPy−OPV−UPy films, for which a similar elastic modulus of 1.5 ± 0.06 GPa was determined by a three-point bending test and a similar mechanical transition was observed above 60 °C by means of dynamic mechanical analysis.[25]

In addition to the above-mentioned experiments with a cold probe and a heated substrate, we used a heated t-SPL probe on a sample at room temperature to test the thermomechanical properties of UPy−OPV−UPy. In particular, the response of UPy−OPV−UPy was tested using the t-SPL's capability to apply heat on a sample area of a few tens to hundreds of square nanometers at extremely high heating rates ranging from 10^5 to 10^8 K/s. In a series of experiments, we measure the indentation depth as a function of probe temperature, indentation force, and heating time. Figure 2b shows a grid of AFM topography images obtained from t-SPL indentation, which were created at tip−sample contact temperatures in the range of 130−310 °C and a tip actuation potential ranging from 6.0 to 9.0 V (indentation force 100−500 nN, see Supporting Information). Two main observations can be made from Figure 2b: first, to thermally modify the supramolecular polymer with the heated probe, a minimum temperature (threshold temperature) is necessary at a given tip actuation potential; second, if the tip actuation potential is below 7.8 V, a pileup is formed, whereas above an additional indent is formed. A small colored bar at the bottom of each topography image in Figure 2b indicates whether an indent (red) or a pileup (blue) is formed. The formation of a pileup without an indent can be attributed to a sufficient high temperature to melt the material but the force is too low to penetrate the material. In Figure 2c, the average indent depth and height of the pileup from 16 indents are plotted as a function of the tip temperature at a tip actuation potential of 7.8 V and a heating time of 8 μs, which is a trade-off value between patterning speed and temperature as will be explained later. The indentation depth increases with temperature above 212 °C and as a consequence the pile-up height increases due to displacement of the molten material. To systematically detect this temperature by AFM, we define a threshold value for the indent depth and pile-up height of 4 times the root-mean-square roughness of the sample topography, which is usually in the range between 3 and 6 nm. The threshold value is chosen sufficiently high to avoid false positive detection of an indent or pileup. The indentation experiment was performed ten times with the same tip on different samples. All patterns were clearly visible and the indents well reproduced. Three experiments out of them were discarded due to surface topography anomalies, which stem from the manual sample fabrication and caused large variations in the data points. These surface irregularities can be avoided in future experiments by using compression molding of UPy−OPV−UPy on a substrate instead of doctor-blading of the melt. In Figure 2d, the average threshold temperature from the seven consecutive indentation experiments is plotted as a function of the indentation force. The temperature necessary to form a modification in the material T_{Thres} decreases linearly with the indentation force F: $T_{\mathrm{Thres}} = T_0 + mF$ with $T_0 = 380$ °C and $m = -0.42$ °C/nN. A linear dependence between threshold temperature and indentation force has been observed for other polymers such as poly(methyl methacrylate) (PMMA) and SU-8.[3] To determine the effect of heating time on the threshold temperature, the tip−substrate contact time was varied over 3 orders of magnitude as shown in Figure 2e. As expected, the temperature required to form an indent decreases with the heating time, known as time−temperature superposition, which is a typical behavior found in polymers. We found that also in supramolecular polymers, which differ

DOI: 10.1021/acsami.7b13672
ACS Appl. Mater. Interfaces 2017, 9, 41454−41461

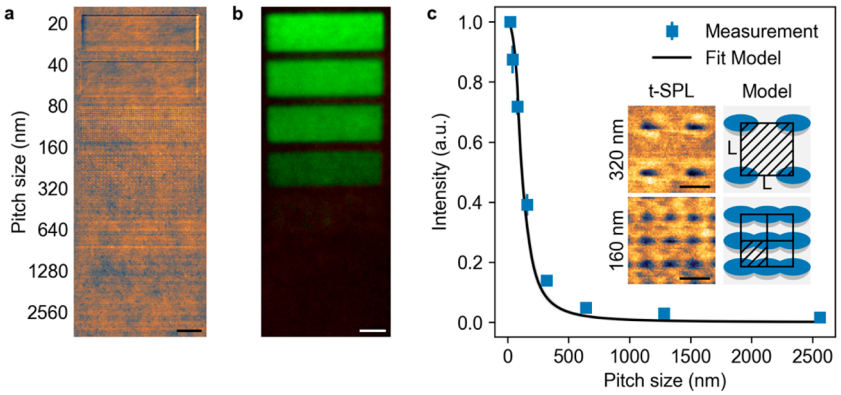

Figure 4. Correlation between fluorescence intensity and pitch size. (a) AFM topography image for different indent pitch sizes varying from 20 nm to 2.56 μm (scale bar 2 μm). (b) Corresponding fluorescence microscopy images acquired under irradiation with UV light (scale bar 2 μm). (c) Plot of the normalized fluorescence intensity as a function of the pitch size. The inset shows the surface topography of indents at a pitch size of 320 and 160 nm and the corresponding model used to fit the green emission per unit area (scale bar 200 nm).

considerably in their molecular assembly from regular polymers, the temperature T at which material softening occurs during thermal indentation can be described by the empirical Williams–Landel–Ferry (WLF) equation: $\ln(t_T/t_r) = -c_1(T - T_r)/(c_2 + (T - T_r))$, with a heating time t_T and a reference time t_r at a reference temperature T_r. The curve was best described with $c_1 = 13.0 \pm 0.4$, $c_2 = 13.1 \pm 3$ °C, and $T_r = 88.0 \pm 4$ °C, whereby similar values have been found for thermal indentation with PMMA and SU-8.[3] By extrapolation of the transition temperature using WLF to long time scales, for example, 1 s, which is comparable to the ones used in AFM spectroscopy, a threshold temperature of 88 °C is obtained. This value is on the same order of magnitude as the glass-transition temperature of UPy–OPV–UPy (73 °C).

Another essential benchmark for UPy–OPV–UPy as a thermal resist is the spatial resolution, which was determined by patterning structures, composed of bars ranging from 1.92 μm in width down to a single line (SL) by consecutive indentation with the heated probe. The maximum resolution is governed by the lateral tip apex diameter (27.7 ± 9 nm), the opening angle (~60°), and the indentation depth (10–30 nm). Figure 3a shows an AFM topography image of the pattern and one can see that a topographic contrast is created between patterned and unpatterned areas. For a line of consecutive indents, a fwhm resolution of 86 ± 6 nm is obtained as shown in the topographical profiles in Figure 3c (black curve). As a comparison, in two-photon laser lithography the voxel size was previously limited to a volume of $3 \times 3 \times 6$ μm^3 due to heat diffusion from the heated spot.[26] In Figure 3c, two noticeable features in the pattern profiles are a trench and a rim that are formed at the left and right side of each structure, respectively. Our observations tell us that this is caused by displacement of molten material through consecutive indentation with the heated probe in the fast-scan direction when the pitch size (20 nm) is smaller than the tip apex diameter. The following mechanism could explain the surface topography reflected by the graph shown in Figure 3c: Starting from the left side, a first indent is formed with the hot probe, and due to volume conservation a rim is formed around the indent. When the pitch size is smaller than the tip, during the consecutive indentation material is displaced into the previous indent and hence no significant depth change can be observed (Figure S4). The pileup of material at the edges is more dominant on the right side than on the left, independent of the width of the structures, which can be explained by the patterning direction of the tip from left to right and the tilt of the cantilever (6° with respect to the substrate surface). After patterning and subsequent AFM microscopy, the sample was analyzed by fluorescence microscopy. In Figure 3b, the corresponding fluorescence microscope image of the t-SPL pattern from Figure 3a is shown. In this image the red fluorescence from the background was suppressed by using a short-pass filter to obtain a better contrast (for an image without filtering see Figure S5). A direct comparison of the resolution between the topography and fluorescence intensity profiles from fluorescence microscopy is not possible due to the diffraction limit of optical microscopes (Figure 3c).

On the basis of the findings above, and to analyze further the achievable limits of the thermal patterning of UPy–OPV–UPy, the correlation between pitch size and pattern quality was investigated. Furthermore, pitch modulation can be used to regulate the green luminescence intensity. Areas of the supramolecular polymer film were written at a pitch size ranging from 20 to 2.56 μm and subsequently imaged directly by the NanoFrazor's probe as shown in Figure 4a. For a pitch size below 80 nm, a trench is formed on the left and a pileup is formed on the right side of the pattern due to the displacement of the melt as already discussed in connection with the data shown in Figure 3a. Above a pitch size of 80 nm, individual indents are distinguishable by AFM and the material displaced during the indentation remains around each indent. The fwhm sizes of the indents are 93 ± 12 and 46 ± 6 nm in the fast-scan direction (horizontal) and in the slow-scan direction (vertical), respectively. A contribution to the asymmetry can be attributed to the tool-specific patterning mechanism of the thermal scanning probe system, whereby the piezo-actuated sample stage is continuously moving in the fast-scan direction at a speed of 0.2 mm/s, while the cantilever is actuated toward the substrate for short indentation times on the order of microseconds. A comparison between the topography and fluorescence image (Figure 4b) reveals that the green fluorescence intensity can be tuned over a broad range by varying the indent density, but the indentation pattern itself is not visible because the t-SPL resolution is higher than the diffraction limit of optical microscopy. In Figure 4c, the normalized fluorescence intensity is plotted as a function of the pitch size, whereby the fluorescence intensity sharply decreases with increasing pitch. For pitch sizes larger than the indent

DOI: 10.1021/acsami.7b13672
ACS Appl. Mater. Interfaces 2017, 9, 41454–41461

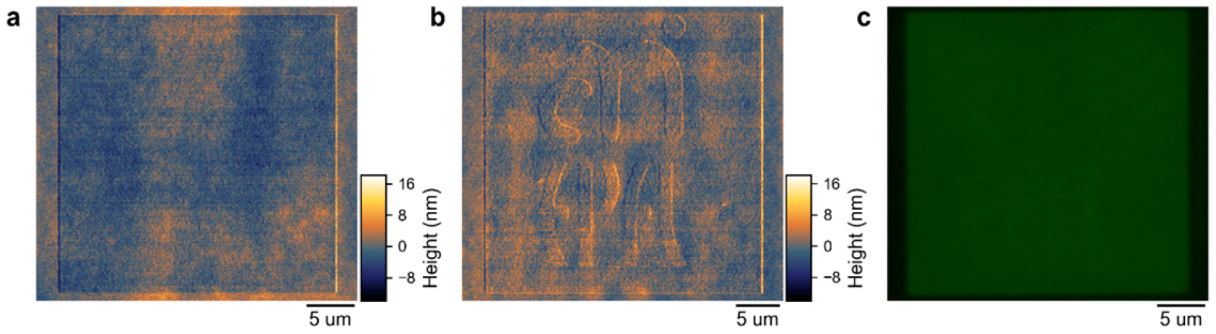

Figure 5. Hidden in plain sight. Thermal patterning of nanoscale features with distinct topography but the same fluorescence intensity. (a) T-SPL patterning of the square of 30 × 30 μm^2 at a pitch size of 60 nm. (b) Overlay of a second t-SPL pattern within the prepatterned square, containing the logos of the two institutes. (c) Fluorescence microscopy image of the patterned area acquired under irradiation with UV light, showing that the features programmed in topology mode are virtually invisible in fluorescence microscopy mode.

length, the intensity is inverse proportional to the square of the pitch size, but as soon as the indents start to overlap, the normalized intensity approaches 1. The inset in Figure 4c shows a magnification of the surface topography with four indents at a pitch size of 320 and 160 nm and a sketch of the model used to fit the fluorescence intensity. In the model it is assumed that the extent of the thermally modified polymer can be approximated with a semiellipsoid with a uniform fluorescence density. The normalized intensity perceivable by fluorescence microscopy is then the ratio between thermally modified volume and the square of the pitch size times the depth of the indent. Details about the model used to fit the fluorescence intensity can be found in the Supporting Information. We fit the measured intensity as a function of pitch size as shown in Figure 4c, whereby only the major axis of the ellipse was used as a fit parameter. The aspect ratio of the indents (r_a = 2.2 ± 0.6) can be determined from the surface topography and should be similar for both, the topological indent and the fluorescent area, due to isotropic spreading of heat. We obtain an indent length of 189 ± 12 nm from the fitted fluorescence curve, which is in agreement with the value obtained by measuring the peak-to-peak indent length from the topography (184 ± 31 nm). From these measurements, we conclude that the disaggregation of the fluorophores due to the heat provided by the tip is confined to only a few nanometers around the indent and the resolution is mainly limited by the tip apex size.

The combination of t-SPL with a color-switchable fluorescent polymer provides the ability to pattern multifaceted nanostructures, which are optically hidden due to the limited contrast or resolution of most optical microscopy systems but topologically detectable with AFM. To demonstrate this, a series of patterns were fabricated with distinct information in the topographic and fluorescent states by way of consecutive patterning steps and readout using both AFM and fluorescence microscopy. First, a square of 30 × 30 μm^2 was patterned with a pitch size of 60 nm (Figure 5a). Subsequently, a second pattern was produced within the square, which can be distinguished from the background by AFM (Figure 5b). However, as shown in Figure 5c, the second pattern is virtually indistinguishable from the background when measured with fluorescence microscopy. To obtain truly hidden features, it is important to avoid deep indents and pileup (Figure S5). To visualize the features with a fluorescence microscope, we choose the hidden t-SPL patterns to be larger than 1 μm, which makes them easily detectable by optical microscopy, whereas in a real security feature the information can be stored in the form of a binary pattern composed of indents and unpatterned areas. For these patterns, we expect an extended lifetime because at room temperature UPy−OPV−UPy is in the glassy state and therefore the particular stacking of the OPV cores—that lead to either green or red fluorescence—is frozen in.

CONCLUSIONS

We have demonstrated nanoscale thermal patterning with a heated probe of a novel thermochromic luminescent supramolecular polymer. t-SPL nanoindentation of thin coatings of UPy−OPV−UPy resulted in a fluorescent as well as a topographical pattern at the nanometer scale on account of a low viscosity above T_g and the ability to kinetically trap a disassembled monomeric state that resulted in a hypochromic shift. In-depth studies of the patterning conditions showed that altering the nanoscale indentation pitch modulated the green fluorescence intensity, material pileup, and overall patterning parameters. This novel coating material combined with the writing parameters could be interesting for application as nano- to micrometer-scale anticounterfeiting features in environments with temperatures not exceeding 180 °C with at least three degrees of security: fluorescence intensity, topography, and the concept of hidden features. Recent advances in laser-assisted and ultrafast nanoimprint lithography could enable mix and match lithography with t-SPL to fabricate large-area patterns in UPy−OPV−UPy which can be locally modified in a subsequent step with a heated probe to create highly customized features that are unique and difficult to reproduce. Furthermore, we anticipate that the presented novel polymer has a broad application beyond patterning by thermal probes such as in temperature, and strain sensing.

ASSOCIATED CONTENT

Supporting Information

The Supporting Information is available free of charge on the ACS Publications website at DOI: 10.1021/acsami.7b13672.

A brief discussion about the diffusion-limited aggregation of OPV, information about the indentation force calibration procedure for thermal cantilevers, the method of evaluation of the indents formed by t-SPL to compute the threshold temperature, thermal patterning, and localizing of the fluorescent structures, a discussion about how the pitch size affects the patterning quality, a detailed description of fluorescence intensity model, unfiltered fluorescence images with red and green

DOI: 10.1021/acsami.7b13672
ACS Appl. Mater. Interfaces 2017, 9, 41454−41461

fluorescence, and a discussion about how hidden features need to be designed to make them invisible with optical microscopes (PDF)

AUTHOR INFORMATION

Corresponding Authors

*E-mail: christoph.weder@unifr.ch.
*E-mail: juergen.brugger@epfl.ch.

ORCID

Samuel Tobias Zimmermann: 0000-0002-2958-5351
Christoph Weder: 0000-0001-7183-1790
Jürgen Brugger: 0000-0002-7710-5930

Present Address

§Department of Bioengineering and Materials Science and Engineering, University of California, Berkeley, Berkeley, CA 94720-1760, USA.

Author Contributions

‖These authors contributed equally to this work. The manuscript was written through contributions of all authors.

Notes

The authors declare no competing financial interest.

ACKNOWLEDGMENTS

The research leading to these results has received funding from the European Research Council under the European Union's Seventh Framework Programme (FP7/2007-2013)/ERC grant agreement no. AdG 291490-MERESPO. This work and equipment were partially supported by the U.S. Army Research Office (W911NF-12-1-0339) and the Swiss National Science Foundation (SNSF) via the R'Equip program (150776), respectively. The authors also thank the SwissLitho AG team for fruitful discussions and for awarding a prize in an idea competition directly related to this publication. The Adolphe Merkle Institute and the EPFL have filed a joint patent application related to some of the processes reported in this manuscript which lists all of the authors as inventors.

REFERENCES

(1) Garcia, R.; Knoll, A. W.; Riedo, E. Advanced Scanning Probe Lithography. *Nat. Nanotechnol.* **2014**, *9* (8), 577−587.
(2) Knoll, A. W.; Pires, D.; Coulembier, O.; Dubois, P.; Hedrick, J. L.; Frommer, J.; Duerig, U. Probe-Based 3-D Nanolithography Using Self-Amplified Depolymerization Polymers. *Adv. Mater.* **2010**, *22* (31), 3361−3365.
(3) Pires, D.; Hedrick, J. L.; De Silva, A.; Frommer, J.; Gotsmann, B.; Wolf, H.; Despont, M.; Duerig, U.; Knoll, A. W. Nanoscale Three-Dimensional Patterning of Molecular Resists by Scanning Probes. *Science* **2010**, *328* (5979), 732−735.
(4) Wei, Z.; Wang, D.; Kim, S.; Kim, S.-Y.; Hu, Y.; Yakes, M. K.; Laracuente, A. R.; Dai, Z.; Marder, S. R.; Berger, C.; King, W. P.; de Heer, W. A.; Sheehan, P. E.; Riedo, E. Nanoscale Tunable Reduction of Graphene Oxide for Graphene Electronics. *Science* **2010**, *328* (5984), 1373−1376.
(5) Neuber, C.; Schmidt, H.-W.; Strohriegl, P.; Ringk, A.; Kolb, T.; Schedl, A.; Fokkema, V.; van Veghel, M. G. A.; Cooke, M.; Rawlings, C.; Dürig, U.; Knoll, A.; de Marneffe, J.-F.; el Otell, Z.; Kaestner, M.; Krivoshapkina, Y.; Budden, M.; Rangelow, I. W. Tailored Molecular Glass Resists for Scanning Probe Lithography. *Proc. SPIE* **2015**, 94250E.
(6) Albisetti, E.; Petti, D.; Pancaldi, M.; Madami, M.; Tacchi, S.; Curtis, J.; King, W. P.; Papp, A.; Csaba, G.; Porod, W.; Vavassori, P.; Riedo, E.; Bertacco, R. Nanopatterning Reconfigurable Magnetic Landscapes via Thermally Assisted Scanning Probe Lithography. *Nat. Nanotechnol.* **2016**, *11* (6), 545−551.
(7) Carroll, K. M.; Lu, X.; Kim, S.; Gao, Y.; Kim, H.-J.; Somnath, S.; Polloni, L.; Sordan, R.; King, W. P.; Curtis, J. E.; Riedo, E. Parallelization of Thermochemical Nanolithography. *Nanoscale* **2014**, *6* (3), 1299−1304.
(8) Shaw, J. E.; Stavrinou, P. N.; Anthopoulos, T. D. High-Speed Scanning Thermal Lithography for Nanostructuring of Electronic Devices. *Nanoscale* **2014**, *6* (11), 5813−5819.
(9) Podpirka, A.; Lee, W.-K.; Ziegler, J. I.; Brintlinger, T. H.; Felts, J. R.; Simpkins, B. S.; Bassim, N. D.; Laracuente, A. R.; Sheehan, P. E.; Ruppalt, L. B. Nanopatterning of GeTe Phase Change Films via Heated-Probe Lithography. *Nanoscale* **2017**, *9* (25), 8815−8824.
(10) Cheong, L. L.; Paul, P.; Holzner, F.; Despont, M.; Coady, D. J.; Hedrick, J. L.; Allen, R.; Knoll, A. W.; Duerig, U. Thermal Probe Maskless Lithography for 27.5 Nm Half-Pitch Si Technology. *Nano Lett.* **2013**, *13* (9), 4485−4491.
(11) Wolf, H.; Rawlings, C.; Mensch, P.; Hedrick, J. L.; Coady, D. J.; Duerig, U.; Knoll, A. W. Sub-20 Nm Silicon Patterning and Metal Lift-off Using Thermal Scanning Probe Lithography. *J. Vac. Sci. Technol., B: Nanotechnol. Microelectron.: Mater., Process., Meas., Phenom.* **2015**, *33* (2), 02B102.
(12) Lisunova, Y.; Spieser, M.; Juttin, R. D. D.; Holzner, F.; Brugger, J. High-Aspect Ratio Nanopatterning via Combined Thermal Scanning Probe Lithography and Dry Etching. *Microelectron. Eng.* **2017**, *180*, 20−24.
(13) Xia, Q.; Keimel, C.; Ge, H.; Yu, Z.; Wu, W.; Chou, S. Y. Ultrafast Patterning of Nanostructures in Polymers Using Laser Assisted Nanoimprint Lithography. *Appl. Phys. Lett.* **2003**, *83* (21), 4417−4419.
(14) Tormen, M.; Sovernigo, E.; Pozzato, A.; Pianigiani, M.; Tormen, M. Sub-100μs Nanoimprint Lithography at Wafer Scale. *Microelectron. Eng.* **2015**, *141*, 21−26.
(15) Yang, L.; Tan, X.; Wang, Z.; Zhang, X. Supramolecular Polymers: Historical Development, Preparation, Characterization, and Functions. *Chem. Rev.* **2015**, *115* (15), 7196−7239.
(16) Webber, M. J.; Appel, E. A.; Meijer, E. W.; Langer, R. Supramolecular Biomaterials. *Nat. Mater.* **2016**, *15* (1), 13−26.
(17) Wang, H.; Ji, X.; Li, Z.; Huang, F. Fluorescent Supramolecular Polymeric Materials. *Adv. Mater.* **2017**, *29* (14), 1606117.
(18) Balkenende, D. W. R.; Olson, R. A.; Balog, S.; Weder, C.; Montero de Espinosa, L. Epoxy Resin-Inspired Reconfigurable Supramolecular Networks. *Macromolecules* **2016**, *49* (20), 7877−7885.
(19) Crenshaw, B. R.; Weder, C. Phase Separation of Excimer-Forming Fluorescent Dyes and Amorphous Polymers: A Versatile Mechanism for Sensor Applications. *Adv. Mater.* **2005**, *17* (12), 1471−1476.
(20) Balkenende, D. W. R.; Monnier, C. A.; Fiore, G. L.; Weder, C. Optically Responsive Supramolecular Polymer Glasses. *Nat. Commun.* **2016**, *7*, 10995.
(21) Sijbesma, R. P.; Beijer, F. H.; Brunsveld, L.; Folmer, B. J. B.; Hirschberg, J. H. K. K.; Lange, R. F. M.; Lowe, J. K. L.; Meijer, E. W. Reversible Polymers Formed from Self-Complementary Monomers Using Quadruple Hydrogen Bonding. *Science* **1997**, *278* (5343), 1601−1604.
(22) Sagara, Y.; Lavrenova, A.; Crochet, A.; Simon, Y. C.; Fromm, K. M.; Weder, C. A Thermo- and Mechanoresponsive Cyano-Substituted Oligo(p-Phenylene Vinylene) Derivative with Five Emissive States. *Chem. - Eur. J.* **2016**, *22* (13), 4374−4378.
(23) Calvino, C.; Neumann, L.; Weder, C.; Schrettl, S. Approaches to Polymeric Mechanochromic Materials. *J. Polym. Sci., Part A: Polym. Chem.* **2017**, *55* (4), 640−652.
(24) Sagara, Y.; Kubo, K.; Nakamura, T.; Tamaoki, N.; Weder, C. Temperature-Dependent Mechanochromic Behavior of Mechanoresponsive Luminescent Compounds. *Chem. Mater.* **2017**, *29* (3), 1273−1278.
(25) Lavrenova, A.; Balkenende, D. W. R.; Sagara, Y.; Schrettl, S.; Simon, Y. C.; Weder, C. Mechano- and Thermoresponsive Photo-

DOI: 10.1021/acsami.7b13672
ACS Appl. Mater. Interfaces 2017, 9, 41454−41461

luminescent Supramolecular Polymer. *J. Am. Chem. Soc.* **2017**, *139* (12), 4302−4305.
(26) Lott, J.; Ryan, C.; Valle, B.; Johnson, J. R.; Schiraldi, D. A.; Shan, J.; Singer, K. D.; Weder, C. Two-Photon 3D Optical Data Storage via Aggregate Switching of Excimer-Forming Dyes. *Adv. Mater.* **2011**, *23* (21), 2425−2429.
(27) Wei, P.; Li, B.; de Leon, A.; Pentzer, E. Beyond Binary: Optical Data Storage with 0, 1, 2, and 3 in Polymer Films. *J. Mater. Chem. C* **2017**, *5* (23), 5780−5786.
(28) Gotsmann, B.; Lantz, M. A.; Knoll, A.; Dürig, U. Nanoscale Thermal and Mechanical Interactions Studies Using Heatable Probes. In *Nanotechnology*; Fuchs, H., Ed.; Nanoprobes; Wiley-VCH Verlag GmbH & Co.: New York, 2009; Vol. *6*, p 121.
(29) Holzner, F. Thermal Scanning Probe Lithography Using Polyphthalaldehyde. Doctoral Thesis, ETH Zürich, Zurich, Switzerland, 2013.
(30) Dürig, U. Fundamentals of Micromechanical Thermoelectric Sensors. *J. Appl. Phys.* **2005**, *98* (4), 044906.

DOI: 10.1021/acsami.7b13672
ACS Appl. Mater. Interfaces 2017, 9, 41454−41461